Modulation instability in waveguides with an arbitrary frequency-dependent nonlinear coefficient

N. Linale,[1,4,*] J. Bonetti,[1,4] A. D. Sánchez,[1,4] S. Hernandez,[2] P. I. Fierens,[3,4] and D. F. Grosz[1,4]

[1]Depto. de Ingeniería en Telecomunicaciones, Centro Atómico Bariloche, Comisión Nacional de Energía Atómica, Río Negro 8400, Argentina
[2]Instituto Balseiro, Universidad Nacional de Cuyo, Bariloche, Río Negro 8400, Argentina
[3]Grupo de Optoelectrónica, Instituto Tecnológico de Buenos Aires, CABA 1106, Argentina
[4]Consejo Nacional de Investigaciones Científicas y Técnicas (CONICET), Argentina
*Corresponding author: nicolas.linale@cab.cnea.gov.ar

In this Letter, we present, for the first time, to the best of our knowledge, the modulation instability (MI) gain spectrum of waveguides with an arbitrary frequency-dependent nonlinear coefficient ensuring strict energy and photon-number conservation of the parametric process. This is achieved by starting from a linear stability analysis of the recently introduced photon-conserving nonlinear Schrödinger equation. The derived MI gain is shown to predict some unique features, such as a nonzero gain extending beyond a zero-nonlinearity wavelength and a complex structure of the MI gain spectrum. Analytical results are shown to be in excellent agreement with numerical simulations.

https://doi.org/10.1364/OL.388677

In the realm of nonlinear optics, modulation instability (MI) is an important process wherefore an intense continuous-wave (CW) optical field propagating in a nonlinear medium breaks up in a train of pulses. In its simplest form, the effect of MI arises as a result of a pump at frequency ω_P generating gain sidebands at the frequencies $\omega_P \pm \Omega$, where Ω is a detuning from ω_P. This configures a particular case of a degenerate four-wave-mixing (FWM) process, where two photons at frequency ω_P are annihilated and two photons at frequencies $\omega_S = \omega_P - \Omega$ and $\omega_{AS} = \omega_P + \Omega$ (Stokes and anti-Stokes sidebands, respectively) are created [1,2], conserving both the energy ($2\hbar\omega_P = \hbar\omega_{AS} + \hbar\omega_S$) and the number of photons, as depicted in Fig. 1.

MI has been studied widely in the area of optical fibers [3] and is related to the formation of optical solitons [4], the generation of coherent light in the infrared [5], and the amplification of FWM interactions in optical communication systems [6], among others. Complete models of MI in waveguides (e.g., [7,8] and references therein) can be used to analyze the interplay between higher-order dispersion, Raman scattering, and self-steepening. The latter arises from the frequency dependence of the nonlinear coefficient of the medium, $\gamma(\omega)$, and is often associated with the breakup of ultrashort pulses upon propagation. It also has profound consequences in the case of the CW pumping of a waveguide, as its inclusion leads to a pump power that maximizes the MI gain [9], and a cutoff power [10,11] above which the MI gain vanishes altogether.

The modeling of MI has been thoroughly analyzed within the framework of the well-known nonlinear Schrödinger equation (NLSE), and its extension including the effects of higher-order dispersion and self-steepening. However, it must be noted that neither the conservation of energy nor the number of photons is guaranteed by the NLSE, even when dealing with lossless waveguides, but for a few cases [12]. In particular, Blow and Wood [13] showed that the energy and the number of photons are simultaneously preserved only in the case where the nonlinear coefficient is given by $\gamma(\Omega) = \gamma_P + \gamma_1^{NLSE}\Omega$, with $\gamma_1^{NLSE} = \gamma_P/\omega_P$.

Recently, we introduced a modified NLSE that conserves both the energy and the number of photons [photon-conserving NLSE (pcNLSE)] for waveguides exhibiting any frequency-dependent nonlinear coefficient, $\gamma(\Omega)$ [14]. This situation can be encountered, for instance, in fibers based on metamaterials such as fibers doped with metal nanoparticles (MNPs). Sipe and Boyd [15] showed theoretically that the inclusion of dopants, such as MNPs, enhances the nonlinearity of the host medium. In Refs. [16–21], Z-scan measurements were performed to obtain the nonlinear refractive index of various compounds containing MNPs of different geometries, sizes, and composition. Since MNPs have strong localized surface plasmonic resonances in the visible and infrared regions, and the corresponding real part of the electrical permittivity is negative [22], Miller's rule [23] states that such doped compounds will present a negative nonlinear refractive index. Consequently, an MNP-doped waveguide may have a negative nonlinear coefficient. In several works [24–27], calculations were made with photonic-crystal fibers (PCFs) doped with silver MNPs. These waveguides exhibit a distinctive zero-nonlinearity wavelength (ZNW)

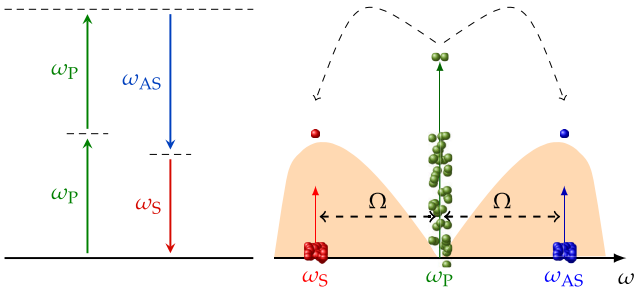

Fig. 1. Modulation instability as a degenerate FWM process. Two photons at the pump frequency are annihilated, and two photons at Stokes and anti-Stokes frequencies are simultaneously created. This process conserves both the energy and the number of photons.

in the near-infrared region. In order to assess the effect of the doping, the propagation of the optical field was approached by resorting to the generalized NLSE with various ways of including the frequency dependence of the resulting nonlinear coefficient. As pointed out, and to the best of our knowledge, an analysis of MI in waveguides with an arbitrary nonlinearity profile has not yet been reported in the framework of photon and energy conservation. In Refs. [28–35], MI analyses up to the second-order nonlinear coefficient were shown in the context of metamaterials. In these works, a typical linear stability analysis [2,36,37] was performed, and the MI gain in metamaterials with a ZNW, g_{MI}, was calculated. However, the number of photons is not preserved, even when neglecting waveguide losses since, as we mentioned before, the NLSE conserves the photon number only when the nonlinear coefficient is a linear function of frequency, with a slope γ_1^{NLSE}.

In this Letter, we derive MI gain profiles starting from the pcNLSE. This propagation equation, based on a simple quantum-mechanical picture of FWM interactions and a generalized Miller's rule [14], reproduces results obtained with the NLSE for a linearly frequency-dependent (with slope γ_1^{NLSE}) nonlinear coefficient, but also allows for the modeling of arbitrary frequency-dependent nonlinear profiles. The pcNLSE in the frequency domain reads

$$\frac{\partial \tilde{A}}{\partial z} = i\beta(\Omega)\tilde{A} + i\bar{\Gamma}(\Omega)\mathcal{F}\left(C^* B^2\right) + i\bar{\Gamma}^*(\Omega)\mathcal{F}\left(B^* C^2\right), \tag{1}$$

where $\tilde{A}$ is the Fourier transform of the complex envelope, $\tilde{B} = \sqrt[4]{\gamma(\Omega)/(\Omega+\omega_P)}\tilde{A}$, $\tilde{C} = (\sqrt[4]{\gamma(\Omega)/(\Omega+\omega_P)})^*\tilde{A}$, and the effective nonlinear coefficient is $\bar{\Gamma}(\Omega) = \sqrt[4]{\gamma(\Omega)(\Omega+\omega_P)^3}/2$. Even though this equation supports any function $\beta(\Omega)$ and $\gamma(\Omega)$, it is usual to work with series expansions:

$$\begin{cases} \beta(\Omega) = \beta_P + \beta_1\Omega + \frac{1}{2}\beta_2\Omega^2 + \cdots, \\ \gamma(\Omega) = \gamma_P + \gamma_1\Omega + \frac{1}{2}\gamma_2\Omega^2 + \cdots. \end{cases} \tag{2}$$

For the linear stability analysis, we start with a CW field $A_P(z) = \sqrt{P_0}e^{ik_P z}$, where P_0 is the pump power, and k_P is the wavenumber, both at frequency ω_P, plus a small perturbation defined as

$$\varepsilon(z, T) = \varepsilon_1 e^{i(Kz-\Omega T)} + \varepsilon_2 e^{-i(Kz-\Omega T)}, \tag{3}$$

such that

$$A(z, T) = A_P(z) + \varepsilon(z, T), \tag{4}$$

where $|\varepsilon| \ll |A_P|$, and K is the wavenumber of the perturbation. By substituting Eq. (4) into Eq. (1), and keeping only first-order terms of the perturbation, the expression for the MI gain is given by

$$g_{MI}(\Omega) = 2\,|\mathrm{Im}\,\{K\}| = 2\left|\mathrm{Im}\left\{\sqrt{\left(\frac{\Delta k}{2}\right)^2 - \bar{\gamma}(\Omega)^2 P_0^2}\right\}\right|, \tag{5}$$

where the mismatch factor, Δk, is defined as

$$\Delta k = 2k_P - k_S - k_{AS} \tag{6}$$

and relates momenta of the interacting photons:

$$\begin{cases} 2k_P = 2\beta_P + 2\gamma_P P_0, \\ k_S = \beta(-\Omega) + 2\bar{\gamma}_S P_0, \\ k_{AS} = \beta(\Omega) + 2\bar{\gamma}_{AS} P_0. \end{cases} \tag{7}$$

The functions $\bar{\gamma}(\Omega)$, $\bar{\gamma}_S(\Omega)$, and $\bar{\gamma}_{AS}(\Omega)$ are defined as

$$\bar{\gamma}(\Omega) = \mathrm{Re}\left\{\sqrt[4]{\gamma_P}\sqrt[4]{\gamma_P}\sqrt[4]{\gamma_S}\sqrt[4]{\gamma_{AS}}\right\}\sqrt[4]{1-(\Omega/\omega_P)^2}, \tag{8}$$

$$\bar{\gamma}_S(\Omega) = \mathrm{Re}\left\{\sqrt[4]{\gamma_S}\sqrt[4]{\gamma_S}\sqrt[4]{\gamma_P}\sqrt[4]{\gamma_P}\right\}\sqrt{1-\Omega/\omega_P}, \tag{9}$$

$$\bar{\gamma}_{AS}(\Omega) = \mathrm{Re}\left\{\sqrt[4]{\gamma_{AS}}\sqrt[4]{\gamma_{AS}}\sqrt[4]{\gamma_P}\sqrt[4]{\gamma_P}\right\}\sqrt{1+\Omega/\omega_P}, \tag{10}$$

where γ_P, $\gamma_S = \gamma(-\Omega)$, and $\gamma_{AS} = \gamma(\Omega)$ represent the nonlinear coefficient at the pump, Stokes, and anti-Stokes frequencies, respectively, as derived from Eq. (2). Note that the separate calculation of the fourth roots is necessary if negative nonlinearities are considered, following the way they are computed in the pcNLSE [14].

From the expressions above, we can calculate the gain spectrum, i.e., the dependence of g_{MI} on frequency. In Fig. 2, profiles of g_{MI} for the NLSE and the pcNLSE are shown, where $\gamma(\Omega)$ is taken as a linear function of frequency, but with an arbitrary value of $\gamma_1 = 10\gamma_1^{NLSE}$, so that the waveguide exhibits a ZNW in the region of interest. For the sake of simplicity, only $\beta_2 < 0$ is taken into account, and higher-order dispersion terms are neglected. Note the differences in MI gain in Figs. 2(a) and 2(b), becoming more apparent as the gain approaches the ZNW. In both cases, and as expected, as $|\beta_2|$ decreases, the gain bandwidth grows. In Fig. 2(c), the gain predicted by the NLSE vanishes altogether, while the pcNLSE predicts a broader gain bandwidth as compared to Figs. 2(a) and 2(b), and also the spectrum exhibits two zero-gain points at each side of the pump.

To validate the analytical results in Fig. 2(c), we performed simulations of Eq. (1) with the same waveguide parameters and pump power. The input field is an intense pump at $\lambda = 800$ nm with a finite optical signal-to-noise ratio of 50 dB (the added noise is circular white Gaussian.) The result of an average over 10 noise realizations is shown in Fig. 3. Note that although there seems to be a discrepancy between the average noise spectral density and the MI gain close to $\Omega = 0$, it can be shown that the former "copies" the shape of the latter only at long propagated distances [38]. Figure 3(a) shows the input and output spectra after propagating 8 L_{MI}, where $L_{MI} = [\max g_{MI}]^{-1}$. In Fig. 3(b), the photon fluxes $\Psi(\omega) = P/\hbar(\omega)$ at frequencies ω_S

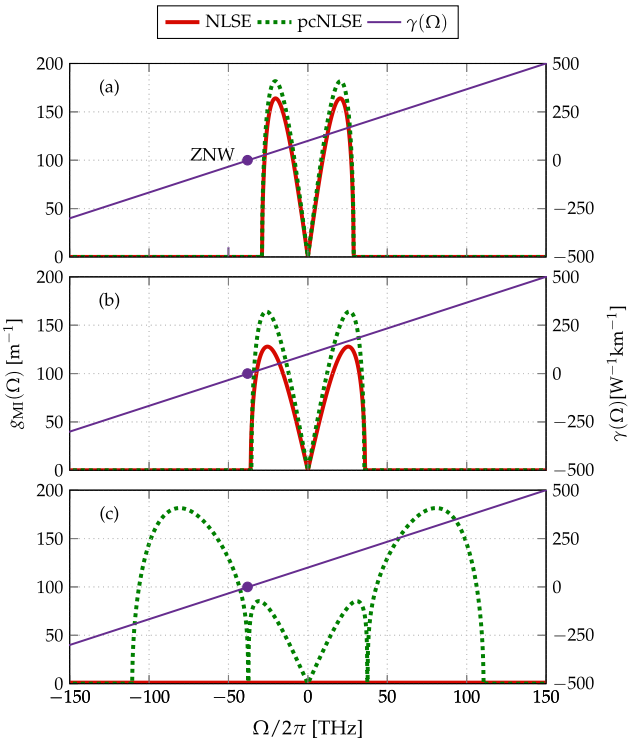

Fig. 2. MI gain profiles for the NLSE (solid line) and the pcNLSE (dashed line). $\gamma(\Omega) = \gamma_{\mathrm{P}} + 10\gamma_1^{\mathrm{NLSE}}\Omega$, with $\gamma_{\mathrm{P}} = 100\ \mathrm{W}^{-1}\ \mathrm{km}^{-1}$, and $P_0 = 1000$ W. (a) $\beta_2 = -10\ \mathrm{ps}^2/\mathrm{km}$; (b) $\beta_2 = -5\ \mathrm{ps}^2/\mathrm{km}$; (c) $\beta_2 = -1\ \mathrm{ps}^2/\mathrm{km}$. The thick dot in the $\gamma(\Omega)$ curve marks the ZNW.

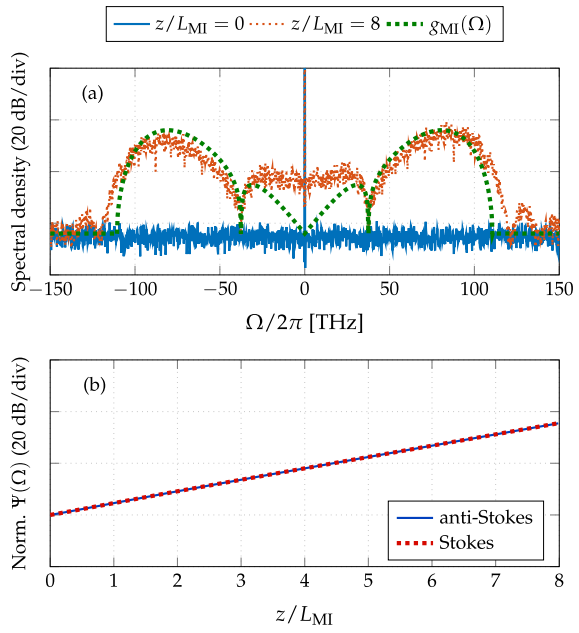

Fig. 3. Simulation results. (a) Input (solid line) and output (dotted line) spectra after propagating a distance proportional to the inverse of g_{MI}. g_{MI} (dashed line) are shown to highlight the region of noise growth. (b) Photon fluxes for Stokes (dashed line) and anti-Stokes (solid line) frequencies.

and ω_{AS}, corresponding to the frequencies of MI gain maxima, are shown. Note that the equal growth of the photon fluxes shows the strict photon-number and energy conservation of the parametric FWM interaction. Further, in Ref. [12], and with an analysis based on the NLSE, it was shown that the equal growth of both sidebands occurs only in the case where $\gamma_1 = \gamma_1^{\mathrm{NLSE}}$. Here, the use of the pcNLSE ensures strict commitment to the parametric FWM interaction for any arbitrary nonlinear profile.

In Ref. [39], the authors show MI gain spectra g_{MI} as a function of the pump power, obtained from the NLSE, and emphasize the existence of a cutoff power [10], defined as $P_{\mathrm{co}}^{\mathrm{NLSE}} = |\beta_2\gamma_{\mathrm{P}}|/\gamma_1^2$ (only β_2 considered), enabled by self-steepening. We define the normalized power as $p = P_0/P_{\mathrm{co}}^{\mathrm{NLSE}}$, so that g_{MI} vanishes when $p > 1$ as predicted by the NLSE. Figure 4 shows g_{MI} profiles as a function of the normalized power, obtained with the pcNLSE, for three different values of γ_1. By varying γ_1 one can readily see that a change in the ZNW towards the pump frequency produces a shift of the points of zero MI gain, leading to a more complex gain structure. In stark contrast, an MI analysis starting from the NLSE (including the effect of self-steepening) yields gain structures like that in the top panel of Fig. 4. Furthermore, the MI gain obtained from the pcNLSE vanishes for $p > 1$ only in the top panel (where $\gamma_1 = \gamma_1^{\mathrm{NLSE}}$). In the middle and bottom panels, the gain extends well beyond the corresponding cutoff power (i.e., there is MI gain for $p > 1$). This explains the vanishing of the NLSE gain in Fig. 2(c): the 1000-W pump power exceeds the cutoff power as obtained with the NLSE, but the pcNLSE predicts a larger cutoff power, and thus the observed MI gain.

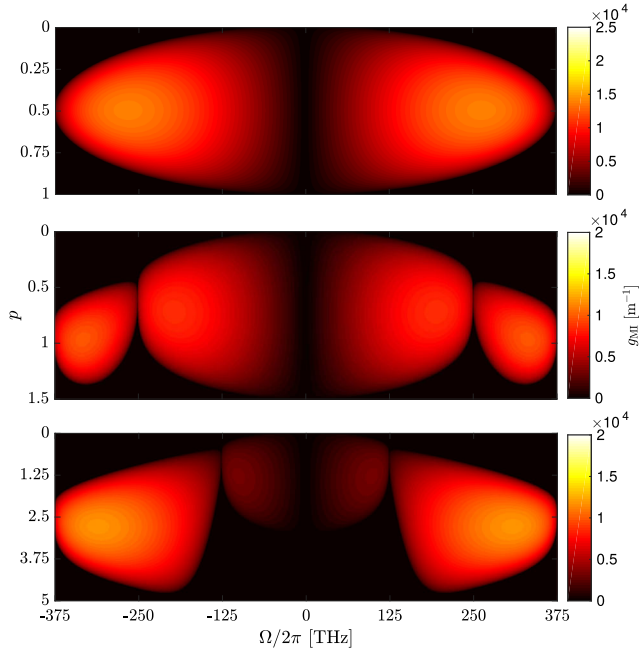

Fig. 4. MI gain profile as a function of Ω and the normalized power $p = P_0/P_{\mathrm{co}}$: (top) $\gamma_1 = \gamma_1^{\mathrm{NLSE}}$; (middle) $\gamma_1 = 1.5\gamma_1^{\mathrm{NLSE}}$; (bottom) $\gamma_1 = 3\gamma_1^{\mathrm{NLSE}}$.

In order to emphasize the complex dependence of the gain spectrum with the nonlinearity profile, Fig. 5(a) shows the MI gain with $p = 2.75$ (same parameters as those from the bottom panel of Fig. 4), and Fig. 5(b) shows the effect of including a quadratic term in the nonlinearity (see, e.g., Ref. [32]) yielding

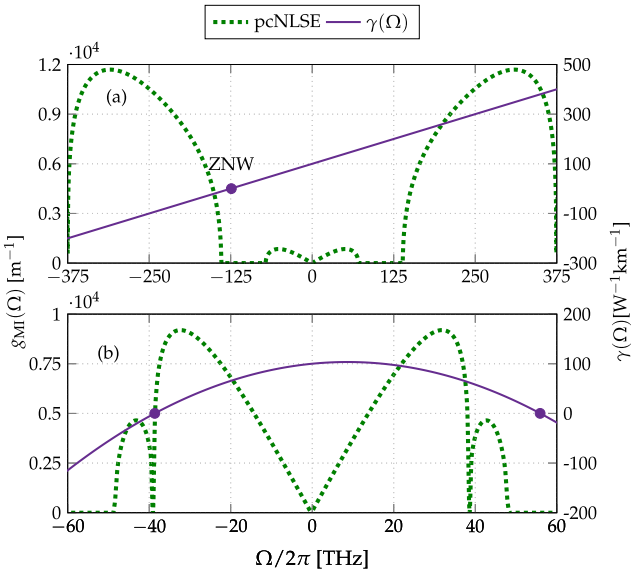

Fig. 5. Modulation instability gain for a linear (a) and a quadratic (b) nonlinearity profile. Zero-nonlinear wavelengths are marked by thick dots.

two ZNWs within the bandwidth of interest. Notice the strong gain compression within a significantly narrower bandwidth in Fig. 5(b) as compared to 5(a) while keeping the same gain amplitude.

In summary, by means of a linear stability analysis of the pcNLSE, we obtained MI gain profiles for waveguides with an arbitrary frequency-dependent nonlinear coefficient, while ensuring strict conservation of the energy and the photon number of the degenerate FWM interaction. The pcNLSE was shown to predict different MI-gain spectra as compared to those obtained with the NLSE, especially so when the zero-nonlinear wavelength of the waveguide lies within the spectral range of interest. In particular, a case was shown where use of the NLSE leads to a vanishing of the MI gain, while the pcNLSE predicts a complex gain spectrum. Numerical simulations, in excellent agreement with analytical results, confirmed these findings. Finally, we believe that the presented MI analysis of the pcNLSE opens the door to easily and correctly tackle nonlinear propagation in interesting media, such as MNP-doped waveguides and, in general, waveguides with frequency-dependent nonlinearities.

Disclosures. The authors declare no conflicts of interest.

REFERENCES

1. V. E. Zakharov and L. Ostrovsky, Physica D **238**, 540 (2009).
2. G. Agrawal, *Nonlinear Fiber Optics, Optics and Photonics* (Academic, 2012).
3. K. Tai, A. Hasegawa, and A. Tomita, Phys. Rev. Lett. **56**, 135 (1986).
4. M. Nakazawa, K. Suzuki, H. Kubota, and H. A. Haus, Phys. Rev. A **39**, 5768 (1989).
5. A. Hasegawa and W. Brinkman, IEEE J. Quantum Electron. **16**, 694 (1980).
6. D. F. Grosz, C. Mazzali, S. Celaschi, A. Paradisi, and H. Fragnito, IEEE Photon. Technol. Lett. **11**, 379 (1999).
7. P. Béjot, B. Kibler, E. Hertz, B. Lavorel, and O. Faucher, Phys. Rev. A **83**, 013830 (2011).
8. J. Bonetti, S. M. Hernandez, P. I. Fierens, and D. F. Grosz, Phys. Rev. A **94**, 033826 (2016).
9. P. K. Shukla and J. J. Rasmussen, Opt. Lett. **11**, 171 (1986).
10. C. D. Angelis, G. Nalesso, and M. Santagiustina, J. Opt. Soc. Am. B **13**, 848 (1996).
11. A. D. Sánchez, S. M. Hernandez, J. Bonetti, P. I. Fierens, and D. F. Grosz, J. Opt. Soc. Am. B **35**, 95 (2018).
12. A. D. Sánchez, P. I. Fierens, S. M. Hernandez, J. Bonetti, G. Brambilla, and D. F. Grosz, J. Opt. Soc. Am. B **35**, 2828 (2018).
13. K. Blow and D. Wood, IEEE J. Quantum. Electron. **25**, 2665 (1989).
14. J. Bonetti, N. Linale, A. D. Sánchez, S. M. Hernandez, P. I. Fierens, and D. F. Grosz, J. Opt. Soc. Am. B **36**, 3139 (2019).
15. J. Sipe and R. W. Boyd, Phys. Rev. A **46**, 1614 (1992).
16. H. Shen, B. Cheng, G. Lu, T. Ning, D. Guan, Y. Zhou, and Z. Chen, Nanotechnology **17**, 4274 (2006).
17. R. Ganeev and A. Ryasnyansky, Appl. Phys. B **84**, 295 (2006).
18. A. Ryasnyanskiy, B. Palpant, S. Debrus, U. Pal, and A. Stepanov, J. Lumin. **127**, 181 (2007).
19. E. Falcão-Filho, C. B. de Araújo, and J. Rodrigues, Jr., J. Opt. Soc. Am. B **24**, 2948 (2007).
20. K.-H. Kim, A. Husakou, and J. Herrmann, Opt. Express **18**, 7488 (2010).
21. H. Zhang, Z. Hu, Z. Ma, M. Gecevičius, G. Dong, S. Zhou, and J. Qiu, ACS Appl. Mater. Interfaces **8**, 2048 (2016).
22. P. B. Johnson and R.-W. Christy, Phys. Rev. B **6**, 4370 (1972).
23. M. Bell, Phys. Rev. B **6**, 516 (1972).
24. S. Bose, A. Sahoo, R. Chattopadhyay, S. Roy, S. K. Bhadra, and G. P. Agrawal, Phys. Rev. A **94**, 043835 (2016).
25. S. Bose, R. Chattopadhyay, S. Roy, and S. K. Bhadra, J. Opt. Soc. Am. B **33**, 1014 (2016).
26. F. Arteaga-Sierra, A. Antikainen, and G. P. Agrawal, Phys. Rev. A **98**, 013830 (2018).
27. S. Bose, R. Chattopadhyay, and S. K. Bhadra, Opt. Commun. **412**, 226 (2018).
28. J. B. Pendry and D. R. Smith, Phys. Today **57**(6), 37 (2004).
29. M. Scalora, M. S. Syrchin, N. Akozbek, E. Y. Poliakov, G. D'Aguanno, N. Mattiucci, M. J. Bloemer, and A. M. Zheltikov, Phys. Rev. Lett. **95**, 013902 (2005).
30. S. Wen, Y. Wang, W. Su, Y. Xiang, X. Fu, and D. Fan, Phys. Rev. E **73**, 036617 (2006).
31. S. Wen, Y. Xiang, W. Su, Y. Hu, X. Fu, and D. Fan, Opt. Express **14**, 1568 (2006).
32. Y. Xiang, S. Wen, X. Dai, Z. Tang, W. Su, and D. Fan, J. Opt. Soc. Am. B **24**, 3058 (2007).
33. S. Wen, Y. Xiang, X. Dai, Z. Tang, W. Su, and D. Fan, Phys. Rev. A **75**, 033815 (2007).
34. Y. Xiang, X. Dai, S. Wen, and D. Fan, J. Opt. Soc. Am. B **28**, 908 (2011).
35. X. Zhong, K. Cheng, and K. S. Chiang, J. Opt. Soc. Am. B **31**, 1484 (2014).
36. W. Shuang-Chun, S. Wen-Hua, Z. Hua, F. Xi-Quan, Q. Lie-Jia, and F. Dian-Yuan, Chin. Phys. Lett. **20**, 852 (2003).
37. M. H. Frosz, T. Sørensen, and O. Bang, J. Opt. Soc. Am. B **23**, 1692 (2006).
38. P. Fierens, S. Hernandez, J. Bonetti, and D. Grosz, "On the spectral dynamics of noise-seeded modulation instability in optical fibers," in *International Conference on Applications in Nonlinear Dynamics* (Springer, 2016), pp. 265–276.
39. S. M. Hernandez, P. I. Fierens, J. Bonetti, A. D. Sánchez, and D. F. Grosz, IEEE Photon. J. **9**, 1 (2017).